

# Pacific sea surface temperature field reconstruction from coral $\delta^{18}\text{O}$ data using reduced space objective analysis

Michael N. Evans,<sup>1</sup> Alexey Kaplan, and Mark A. Cane<sup>2</sup>

Lamont-Doherty Earth Observatory, Palisades, New York, USA

Received 5 September 2000; revised 25 July 2001; accepted 20 September 2001; published 27 February 2002.

[1] A systematic methodology for the reconstruction of climate fields from sparse observational networks of proxy data, employing the technique of reduced space objective analysis, is applied to the reconstruction of gridded Pacific Ocean Basin sea surface temperature (SST) from coral stable isotope ( $\delta^{18}\text{O}$ ) data for the period 1607–1990. In this approach we seek to reconstruct only the leading modes of large-scale variability which are both observed in the modern climate and resolved in the proxy data. We find that the coral data verifiably resolve two spatial patterns of SST variability. The first and dominant pattern is that of the El Niño–Southern Oscillation (ENSO). A second pattern reflects uniform changes over most of the Pacific Basin. Calibration and verification tests for 1856–1990 show that root-mean-square variance is small ( $\leq 0.5^\circ\text{C}$  RMS) and reconstruction errors are large ( $\leq 0.6^\circ\text{C}$  RMS), limiting interpretation to the tropical region. Periods of enhanced ENSO activity similar to those observed in the past two decades are evident in the reconstruction for the early nineteenth century. The changing frequency of ENSO warm phase events appears to coincide with warming of the Pacific mean state inferred from similar reconstruction efforts using tree ring indicators over the last two centuries. *INDEX TERMS:* 3344 Meteorology and Atmospheric Dynamics: Paleoclimatology; 4215 Oceanography: General: Climate and interannual variability (3309); 4522 Oceanography: Physical: El Niño; *KEYWORDS:* objective analysis, ENSO, sea surface temperature, proxy, coral

## 1. Introduction

### 1.1. Motivation

[2] The motivation for this work is the desire to understand the natural variability of the climate system on timescales from years to centuries and place the somewhat unusual last few decades within a longer-term context. However, our direct (or instrumentally recorded) observations of most climate variables only extend back for about 100–150 years. In their absence we call upon high-resolution paleoproxy data, that is, observations of parameters which vary in a way we understand with the climate variable of interest, to study preinstrumental and pre-industrial climates.

[3] Now, suppose we think of the climate system as consisting of only a handful of patterns superimposed upon one another, which together describe some sizable fraction of the large-scale, low-frequency variability [Wallace, 1996a, 1996b]. Some examples of such patterns in today's climate are the influences of the El Niño–Southern Oscillation (ENSO) phenomenon [Philander, 1990], near-global temperature trends [Hansen and Lebedeff, 1988; Cane *et al.*, 1997], Pacific and Atlantic Basin centered decadal phenomena such as the Pacific Decadal Oscillation [Zhang *et al.*, 1997] and the North Atlantic Oscillation [Hurrell, 1995], and interannually varying Antarctic circumpolar waves [White and Peterson, 1996]. If the patterns are indeed few, important, and large scale, then we might be able to monitor them using only a handful of well-located direct observations [Bretherton and McWilliams, 1980; Bennett, 1990; Jones *et al.*,

1997; Evans *et al.*, 1998]. We may even be able to reconstruct past climatic variability using an observational antenna composed of proxy data.

[4] Our methodological basis for climate field reconstructions follows from recently developed reduced space objective analysis procedures for the analysis of historical climate fields [Cane *et al.*, 1996; Kaplan *et al.*, 1997, 1998; Evans *et al.*, 2001; Kaplan *et al.*, 2000]. In this approach we seek to reconstruct only the leading modes of large-scale variability (space reduction) which are both observed in the modern climate and resolved in the proxy data, given uncertainties [Evans *et al.*, 2001].

[5] At all stages we emphasize the following.

1. The proxy data are permitted to provide climatic information in regions far removed from the sampling site (globality).
2. The proxy data are employed within the context of their observational errors, which are determined via calibration studies (objectivity).
3. All statistical estimates made during analysis are filtered to bring out the most robustly resolved features (space reduction). The relationship of the proxy data to climate variability is treated similarly.

[6] Given explicit assumptions, the analysis produces fields and error estimates. The results may be subsequently checked for consistency with parameter choices and procedural assumptions by comparison with direct and proxy observations not used in the reconstruction procedure and with results from benchmark experiments.

[7] Here we attempt reconstruction of the Pacific Basin sea surface temperature (SST) field using the coral stable isotope ( $\delta^{18}\text{O}$ ) data set studied by [Evans *et al.*, 2000]. We begin by giving an overview of the methodology (section 2), which is developed in detail elsewhere [Evans *et al.*, 2001]. The SST field reconstruction builds on previous work [Evans *et al.*, 2000] which sought to determine which, if any, large-scale patterns of SST variability are resolved by the coral data (section 3.3). We conclude by comparing the results with SST reconstructions based on tree ring-derived indicators from the Pacific coasts of North and South America

<sup>1</sup>Now at Laboratory of Tree-Ring Research, University of Arizona, Tucson, Arizona, USA.

<sup>2</sup>Also at Department of Earth and Environmental Sciences, Columbia University, New York, New York, USA.

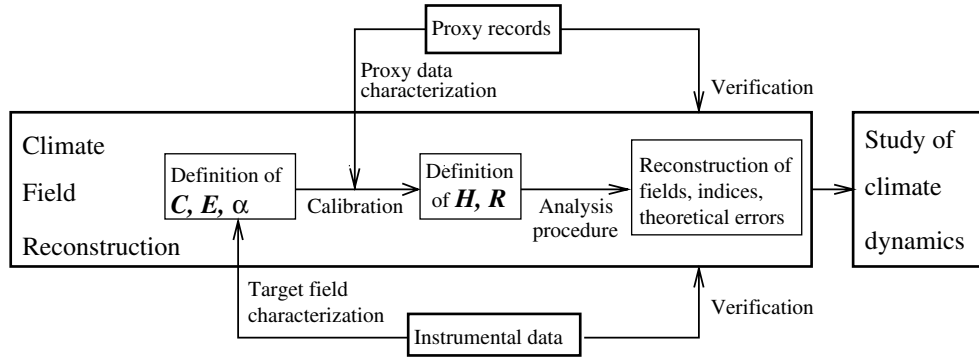


**Figure 1.** Methodology of objective analysis climate field reconstruction from proxy data.

[Evans *et al.*, 2001] and comment on the behavior of the ENSO system inferred from these results.

## 2. Methodology

[8] Our objective is to obtain the linear least squares fit to available observations and a model of the large-scale modes of spatial field variation. The procedure is schematically diagrammed in Figure 1 and described briefly below. More details are given by Evans *et al.* [2001].

### 2.1. Target Climate Field

[9] Missing observations, changes in measurement protocols and quality, and other factors introduce uncertainty in all geophysical data sets. Hence we begin with analysis of the historical observations of the climate field we seek to reconstruct to emphasize the largest-scale features which are likely to have the smallest relative errors. This is conveniently performed using empirical orthogonal function (EOF) analysis, which decomposes the spatial covariance of the climate field  $\mathbf{T}(\mathbf{x}, \mathbf{t})$  into a set of orthogonal vectors and their corresponding variances:

$$\mathbf{C} = \langle \mathbf{T}\mathbf{T}^T \rangle \approx \mathbf{E}\mathbf{\Lambda}\mathbf{E}^T, \quad (1)$$

where boldface variables indicate vectors or matrices, quantities within angle braces are time-averaged, and in all equations hereafter, superscript  $T$  denotes the matrix or vector transpose. Here  $\mathbf{E}$  is a matrix whose columns are a small number of the eigenvectors of  $\mathbf{C}$ , and  $\mathbf{\Lambda}$  is a square matrix whose diagonal elements are the eigenvalues corresponding to  $\mathbf{E}$ . We then assume a reduced space form for the reconstruction solution:

$$\mathbf{T}(\mathbf{x}, \mathbf{t}) = \mathbf{E}(\mathbf{x})\boldsymbol{\alpha}(\mathbf{t}) + \text{residual}, \quad (2)$$

where  $\mathbf{T}$  is the matrix whose rows are time series of climatic observations, with each row corresponding to a location, and  $\boldsymbol{\alpha}(\mathbf{t})$  is the low-dimensional vector of amplitudes with which the modes  $\mathbf{E}$  contribute to the climate field  $\mathbf{T}$ . The long-term mean of  $\mathbf{T}$  is zero.  $\mathbf{E}$ ,  $\boldsymbol{\alpha}$ , and  $\mathbf{T}$  are estimated from the modern observations and provide the basis for calibration of the proxy data.

### 2.2. Calibration

[10] We next choose a set of paleoproxy observations suitable for the reconstruction of the target climate field and calibrate the proxy data over some contemporaneous time interval. Note that by calibrating the proxy data in terms of the large-scale patterns identified in the modern climate observations, we permit the proxies to describe nonlocal as well as local climate variability. For instance, a proxy climate data set including observations from the eastern equatorial Pacific will likely permit calibration of (at

least) the large-scale ENSO climate pattern. We write

$$\mathbf{D}(\mathbf{t}) = \mathbf{H}\boldsymbol{\alpha}(\mathbf{t}). \quad (3)$$

The measurement operator  $\mathbf{H}$  represents a linear relationship between the climate field and proxy observations. If  $\mathbf{H}$  is known, (3) sets up a Gauss-Markov observational scheme for estimation of  $\boldsymbol{\alpha}(\mathbf{t})$  from the matrix of proxy observations  $\mathbf{D}$  [Gandin, 1965; Mardia *et al.*, 1979; Rao, 1973]. Note that there are important assumptions and caveats in this approach; see sections 2.3.1 and 2.3.2 for discussion. We use the proxy data and modern climate observations to estimate  $\mathbf{H}$  over a calibration interval, using the singular value decomposition (SVD) [Bretherton *et al.*, 1992; Fritts *et al.*, 1971; Cook *et al.*, 1994] to regress the proxies on only the leading patterns in the modern observations. The error variance in the model (equation (3)) is estimated from the covariance matrix of the proxy-climate calibration discrepancy:

$$\mathbf{R} = \langle (\mathbf{D} - \mathbf{H}\boldsymbol{\alpha})(\mathbf{D} - \mathbf{H}\boldsymbol{\alpha})^T \rangle. \quad (4)$$

### 2.3. Analysis

[11] We now seek the field  $\mathbf{T}(\mathbf{x}, \mathbf{t})$  which is the best fit to the calibrated proxy observations and to the set of leading patterns we observe in the modern climate, given uncertainty. We construct a cost function:

$$\mathbf{S}(\boldsymbol{\alpha}) = (\mathbf{H}\boldsymbol{\alpha} - \mathbf{D})^T \mathbf{R}^{-1} (\mathbf{H}\boldsymbol{\alpha} - \mathbf{D}) + \boldsymbol{\alpha}^T \mathbf{\Lambda}^{-1} \boldsymbol{\alpha} \quad (5)$$

where  $S$  evaluated at each time  $t$  is a unitless scalar quantity. Here  $\boldsymbol{\alpha}$  is the vector of temporal amplitudes we seek to reconstruct from the proxy data. The first term of (5) represents the misfit of the reconstruction to the calibrated observations and is weighted by the calibration error. The second term represents the misfit to the modern climatology and is weighted by the covariance of the modern climate signal. At each time  $t$  the analysis is punished ( $S \rightarrow$  large) for either putting too much stock in observations with large error or in patterns which explain little of the variance in the modern climate. If the proxy observations and statistical climate model errors are unbiased and if the prior covariances  $\mathbf{C}$ ,  $\mathbf{R}$ , and  $\mathbf{\Lambda}$  are good estimates of the true covariances, then minimization of (5) produces the optimal least squares reduced space estimate of  $\boldsymbol{\alpha}$  [Kaplan *et al.*, 1997]:

$$\boldsymbol{\alpha} = \mathbf{P}\mathbf{H}^T \mathbf{R}^{-1} \mathbf{D}. \quad (6)$$

The error covariance in the estimate is

$$\mathbf{P} = (\mathbf{H}^T \mathbf{R}^{-1} \mathbf{H} + \mathbf{\Lambda}^{-1})^{-1}, \quad (7)$$

**Table 1.** Coral  $\delta^{18}\text{O}$  Records Employed in This Work<sup>a</sup>

Site	Name	Location	Time Period	Genus	Reference
Aqaba	AQ18	29.5°N, 35°E	1788–1992:A	<i>Porites</i>	<i>Heiss</i> [1994]
Aqaba	AQ19	29.5°N, 35°E	1886–1992:A	<i>Porites</i>	<i>Heiss</i> [1994]
Cebu	CEB	10°N, 124°E	1859–1979:A	<i>Porites</i>	<i>Patzöld</i> [1984]
Secas Island	SEC	8.0°N, 82.0°W	1708–1984:M	<i>Porites</i>	<i>Linsley et al.</i> [1994]
Kiritimati	KIR	2°N, 157°W	1938–1993:M	<i>Porites</i>	<i>Evans et al.</i> [1999]
Tarawa Atoll	TAR	1°N, 172°E	1894–1989:M	<i>Porites</i>	<i>Cole et al.</i> [1993]
Urvina Bay	URV	0.4°S, 91.2°W	1607–1953,62-81:A	<i>Pavona</i>	<i>Dunbar et al.</i> [1994]
Punta Pitt	PUN	0.7°S, 89°W	1936–1983:S	<i>Pavona</i>	<i>Shen et al.</i> [1992]
Mahe, Seychelles	MAH	4.6°S, 55.8°E	1846–1995:M	<i>Porites</i>	<i>Charles et al.</i> [1997]
Madang, PNG	MAD	5.2°S, 145.9°E	1922–1991:S	<i>Porites</i>	<i>Tudhope et al.</i> [1995]
Espiritu Santo	ESP	15°S, 167°E	1806–1979:A	<i>Platygyra</i>	<i>Quinn et al.</i> [1993]
New Caledonia	CAL	20.7°S, 166.2°E	1660–1991:S	<i>Porites</i>	<i>Quinn et al.</i> [1998]
Abraham Reef	ABR	22°S, 153°E	1635–1957:B	<i>Porites</i>	<i>Druffel and Griffin</i> [1993]

<sup>a</sup>Nominal temporal resolution of  $\delta^{18}\text{O}$  data: M, monthly; S, seasonal; A, annual; B, biennial. Sites are ordered in decreasing latitude (north to south).

which is a weighted average of the error in the calibrated observations and the error in our model of the modern climate. When the observations are relatively accurate ( $\mathbf{R}$  is small) or sufficiently numerous (the patterns in  $\mathbf{H}$  are well resolved), the analysis error (7) is low, and the analysis puts variance into the solution  $\mathbf{T}$ . When the observations are poor ( $\mathbf{R}$  is large) or absent ( $\mathbf{H}$  is ill resolved), the analysis error becomes large, and the resolved variance approaches climatology or the trivial solution  $\mathbf{T} = \mathbf{0}$ . Similarly, if the relationship between proxy data and direct observations has little skill, the calibration error covariance  $\mathbf{R}$  will be large, the number of calibrated patterns contained in  $\mathbf{H}$  will be small, the analysis error  $\mathbf{P}$  will be large, and the analysis estimate  $\alpha$  will be small. In all cases the paleoclimate estimate  $\alpha$  is constructed in such a way to be consistent with the prior estimates of uncertainty and with the changing availability of proxy data over time.

**2.3.1. Assumptions.** [12] At this stage we summarize the assumptions of the methodology.

1. The analysis of modern climate variability produces unbiased estimates of  $\mathbf{E}$ ,  $\alpha$ ,  $\mathbf{A}$ , and  $\mathbf{T}$ . All errors are random.

2.  $\mathbf{E}$ , which is based on modern observations, describes the patterns of climatic variability recorded in the paleoproxy data. Linear combinations of the columns of  $\mathbf{E}$  may be used to describe the fields observed via the proxy data.

3. Errors in the modern observations are small relative to those in the proxy data.

4. The relation between climatic patterns and the proxy data is linear about the mean value; in other words, proxy observations are unbiased estimates of the targeted climate variable to be reconstructed or else are linearly related to a parameter which covaries with the target climate field [*Evans et al.*, 2000].

5. The estimate of this calibration relationship  $\mathbf{H}$  and the covariance of the model residual  $\mathbf{R}$ , which are developed over a specified calibration interval, are unbiased, correct, and constant.

6. There is no age model error in the annually averaged proxy data.

**2.3.2. Caveats.** [13] Shortcomings of the approach are described below.

1. Space reduction (EOF filtering) emphasizes common features expressed across target climate field and the proxy data set, which we expect to be climatic in origin. It discounts both climatic and proxy variability, which explains little common variance, and is most likely to be dominated by observational errors. However, since the historical observations and the proxy data are not spatially and temporally complete, estimates of EOFs and principal components may be affected by selection bias [*Lawley*, 1956; *Schneider*, 2001].

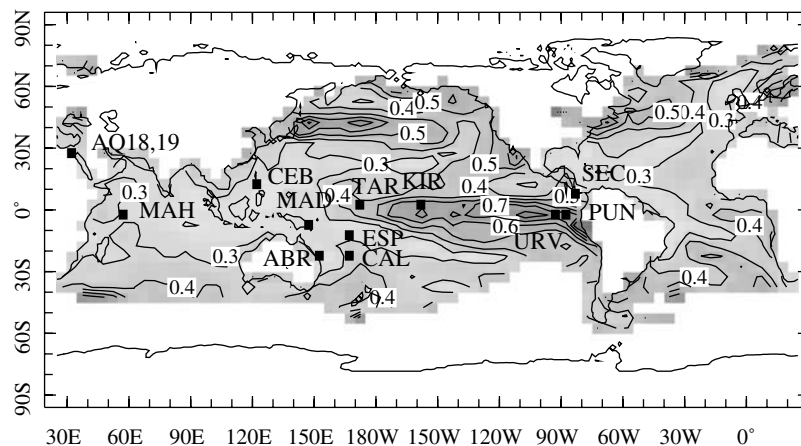


**Figure 2.** Sampling sites for the 13 coral data sets examined in this study. Contours give the RMS SST anomaly from the *Kaplan et al.* [1998] analysis (contour interval is  $0.1^\circ\text{C}$ ). Site names are abbreviated as in Table 1. The reconstruction domain will be the region  $110^\circ\text{E}$ – $70^\circ\text{W}$ .

2. In practice, the small number of available proxy data sets limits the number of patterns which may be calibrated. Hence it is likely that past climate variability, as represented by the proxy observations, is not spanned by the calibrated patterns.

3. We assume that all errors in historical observations and in the proxy data are random. This is most certainly not the case. For instance, changes in observational methods and in the distribution of observations over time in historical observations are typical in many types of climatic variables [e.g., see *Parker et al.*, 1994; *Hansen and Lebedeff*, 1988]. Proxy data often have analogous error sources as well as uncertainty in the interpretation of the proxy measurement and in age model development. See below for a discussion of the problem of age model error in the proxy data.

4. Proxy observations are not always unbiased or linear estimates of climate variables.

5. The number of patterns calibrated (rank of **H**) involves a somewhat subjective choice by the investigator. In principle, this can give rise to overcalibration. The influence of potential overcalibration problems may be examined using verification tests such as those described in section 2.4. See section 4 for an argument that given the features of the methodology presented here, this introduced subjectivity has minimal influence on the results.

6. We assume that there are no errors in the assignment of time to proxy records, but this cannot be true since time is never measured directly, only inferred, in such records. Random or systematic age model errors in individual coral data sets must introduce errors in the reconstructions. In the approach described here they do so implicitly by degrading the calibration estimate with random error or bias, increasing the calibration uncertainty, and offsetting timing of reconstructed events, resulting in degraded reconstructions.

#### 2.4. Verification

[14] The final stage of the procedure is testing of the analysis results for consistency with prior estimates, assumptions, and independent observations. We may test the results by comparison of the proxy-reconstructed climate estimates with (1) historical climate observations not used in calibration of the proxy data, (2) proxy observations not employed in the reconstruction, (3) reconstructed climate based on synthetic proxy data (these synthetic data may be historical climate observations chosen to mimic the expected qualities of the real proxy data or red noise time series with the autocovariance statistics of the real proxy data), and (4) other proxy-based reconstructions of past climates produced from independent data sets. Once the strengths and weaknesses of the reconstruction are clearly known, we may proceed to the study of the reconstructed climate variability.

### 3. Pacific SST Field Reconstructions from Coral $\delta^{18}\text{O}$ Data

#### 3.1. Target Climate Field

[15] As an example of the methodology described in section 2, we reconstruct the Pacific Basin sea surface temperature field, using 13  $\delta^{18}\text{O}$  time series derived from reef corals collected from 12 tropical Pacific, Indian Ocean, and Red Sea sites (Table 1). These same data were systematically compared with analyzed instrumental SSTs by *Evans et al.* [2000]. We choose Pacific SSTs as a target climate field for its importance to global atmospheric circulation and climate anomalies [*Glantz et al.*, 1990].

[16] Our description of historical SST variability is based on the analysis of [*Kaplan et al.*, 1998] of the MOHSST5 [*Parker et*

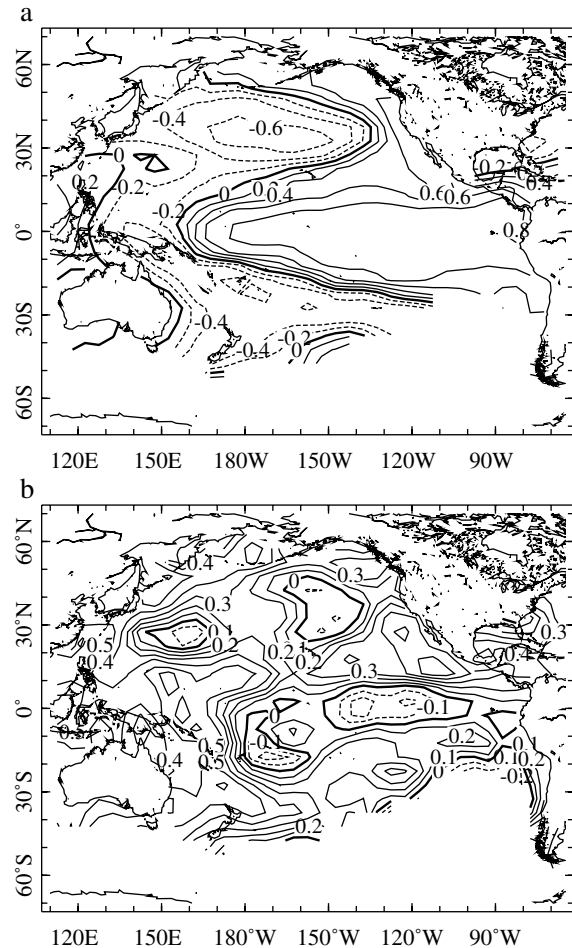


**Figure 3.** (a) Reconstructed spatial pattern 1, illustrated as the correlation of the SST field [*Kaplan et al.*, 1998] with the time series of the two calibrated patterns over the calibration period, 1923–1990. Contour interval is 0.2. (b) Same as in Figure 3a, except for reconstructed spatial pattern 2; contour interval is 0.1.

*al.*, 1994] product of the U.K. Meteorological Office. MOHSST5 is a  $5^\circ \times 5^\circ$  monthly compilation of historical (1856–1991) ship-based observations of SST, quality-controlled for obvious outliers and corrected for estimated observational biases. The analysis of this observational data set employs the newly developed technique of the reduced space optimal smoother to objectively extract large-scale variations of SST on a near-global grid ( $40^\circ\text{S}$ – $60^\circ\text{N}$ ) from incomplete spatial and temporal observations. The small-scale features of SST variability, totaling  $0.3$ – $0.4^\circ\text{C}$  in average amplitude and not constrained by modern high quality observations, are filtered out in this approach. *Kaplan et al.* [1997, 1998] discuss the approach in detail, providing error estimates, numerous verification exercises, and tests of the robustness, strengths, and limitations of the analyzed fields. For our purposes we will seek reconstruction of annual (April to March) mean SST, as this definition is a “natural” climate year for tropical phenomena expected to be resolved in the coral data [*Ropelewski and Halpert*, 1987]. Hereafter we will refer to these annually averaged anomalies as KaSSTa. While we believe this product is a good description of historical interannual and longer-term, large-scale SST variability, no existing historical analysis of global SST fields is free of problems owing to severe data

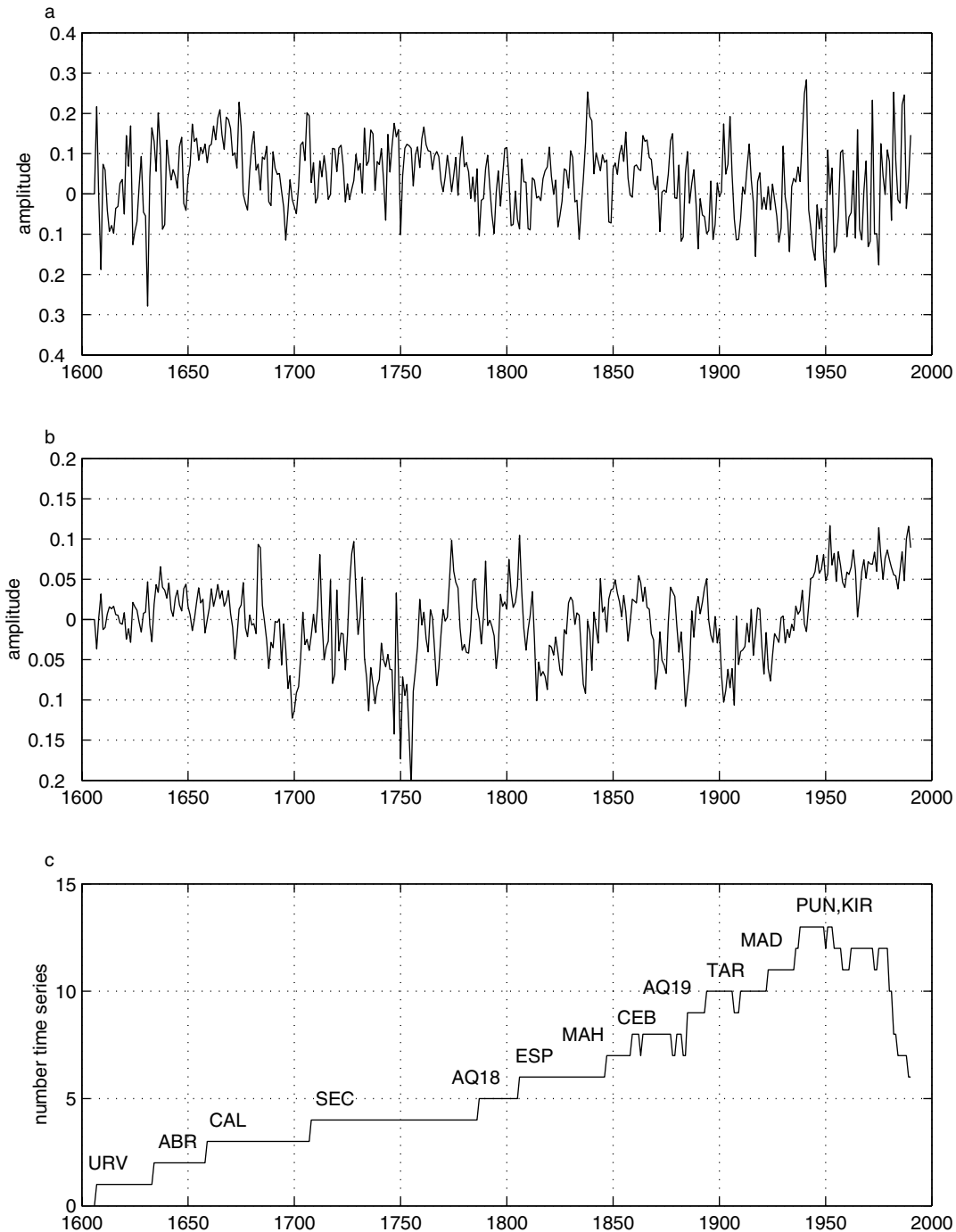


**Figure 4.** (a) Time series of reconstructed pattern 1. (b) Time series of reconstructed pattern 2. (c) Number of coral time series available. Abbreviations for coral names as in Table 1; position of label shows approximate start time of individual coral time series.

deficiencies [Hurrell and Trenberth, 1999]. Specific problems and prospects of the analysis techniques used here are discussed by Kaplan *et al.* [2002].

### 3.2. Proxy Data

[17] Many high-resolution paleoclimatic studies have exploited coral  $\delta^{18}\text{O}$  measurements to construct decades- to centuries-long records of tropical near-surface conditions. The oxygen isotopic composition of coralline aragonite is an

approximately linear function of the SST in which the coral secretes its aragonite, the local net freshwater flux, and a disequilibrium offset from sea water  $\delta^{18}\text{O}$ . In a previous paper [Evans *et al.*, 2000] we argued that such data could be used together to study large-scale patterns of SST variability, through resolution of the covariant local SST or local sea water  $\delta^{18}\text{O}$  signal recorded by the corals. Here we employ the same 13 coral data set studied in our previous work. These records are listed in Table 1, and their locations are shown in Figure 2.

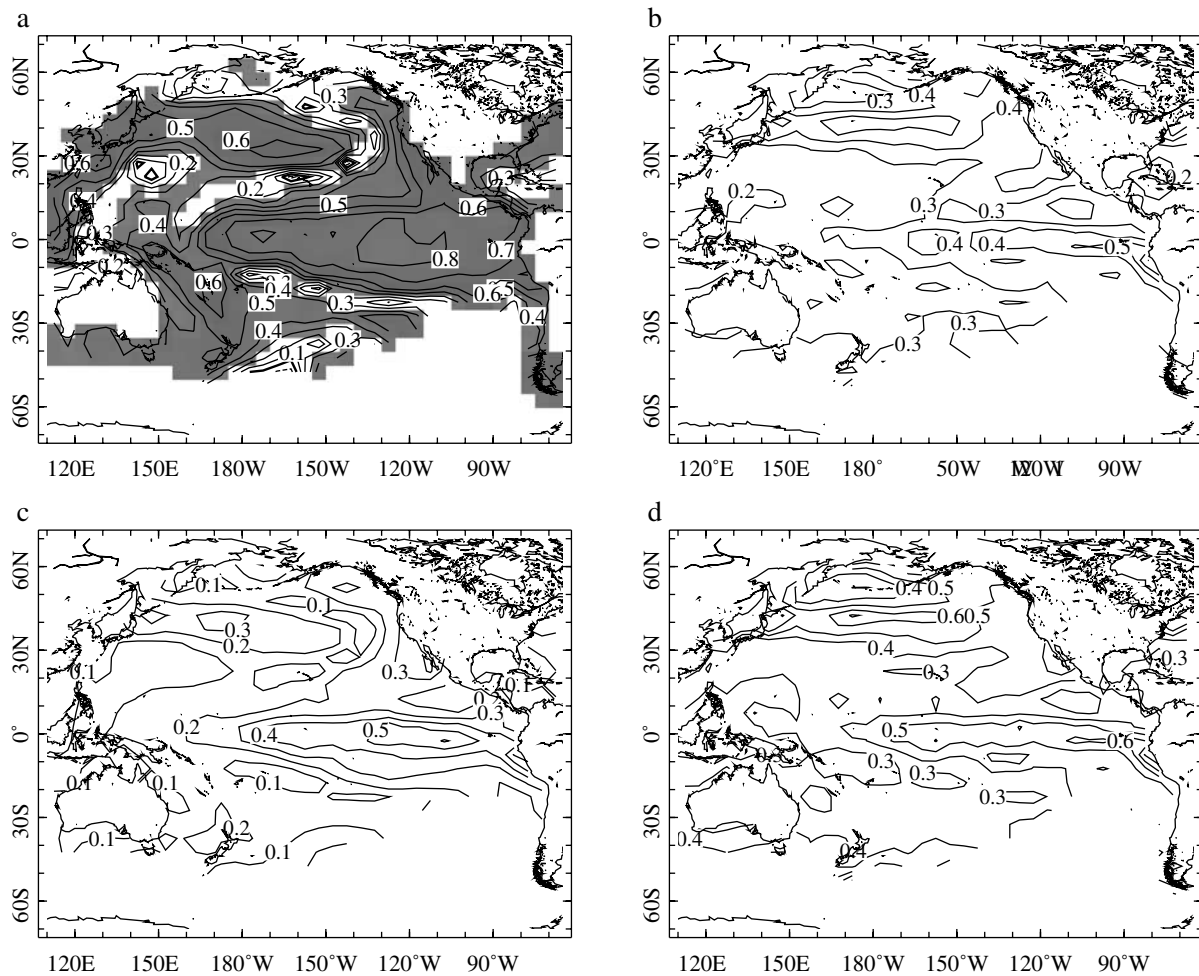


**Figure 5.** Calibration (1923–1990) statistics for the coral-based SST reconstruction (CoSSTa). (a) Correlation. Shading indicates significance at the 95% confidence level, assuming 44 effective degrees of freedom. (b) Root-mean-square difference between CoSSTa and historical SST [Kaplan *et al.*, 1998] ( $^{\circ}\text{C}$ ). (c) Mean amplitude of CoSSTa ( $^{\circ}\text{C}$ ). (d) Estimated error in CoSSTa ( $^{\circ}\text{C}$ ).

Reported resolution of the records vary from monthly (TAR, KIR, MAH, and SEC) to seasonal (MAD, CAL, and PUN) to annual (AQ18, AQ19, CEB, URV, and ESP) to biennial (ABR). We calculate anomalies relative to the seasonal cycle (if any is resolved) in the data and average each record to annual (April–March mean) resolution.

### 3.3. Calibration

[18] We calibrate the coral  $\delta^{18}\text{O}$  data using KaSSTa. To provide for testing of the results, the potential full calibration period (1856–1990) was split into two halves of equal length (1923–1990 and 1856–1922). The coral  $\delta^{18}\text{O}$ -based reconstruction was made using the calibration interval 1923–1990. The complementary period (1856–1922) was reserved for verification (section 2.4). Hereafter we refer to the coral-based SST reconstruction as CoSSTa. Results of the calibration were consistent with Evans *et al.* [2000], who argued that two patterns could be verifiably resolved from the thirteen coral time series.

### 3.4. Analysis

[19] Reconstruction was performed for the interval 1607–1990, over which at least one coral time series was available. The spatial patterns which were reconstructed are shown in Figure 3 as the

correlation of the SST field with the time series of the two calibrated patterns over the calibration period, 1923–1990. The time series of the reconstructed patterns together with the number of coral time series available for analysis are shown in Figure 4. Consistent with the results of Evans *et al.* [2000], the two patterns look like the oceanographic signature of the ENSO phenomenon (Figure 3a) and a basin-wide positive trend, in which portions of the eastern equatorial and North Pacific show the opposite sense (negative) trend (Figure 3b).

[20] To check our initial assumptions (section 2.3.1), we show four field statistics comparing CoSSTa to KaSSTa (Figures 5–9). Correlation between CoSSTa and KaSSTa shows where the calibrated patterns have skill, regardless of signal amplitude (Figures 5a–9a). The root-mean-square difference between CoSSTa and KaSSTa gives the mean actual error in the reconstructed fields (Figures 5b–9b). Figures 5c–9c shows the RMS variance of CoSSTa; this map may be compared to Figure 2 to assess the extent to which the analysis resolves variance in the target climate field. Figures 5d–9d gives the estimated error in CoSSTa, calculated from the error covariance matrix  $\mathbf{P}$  (equation (7)) as  $\text{diag}(\mathbf{EPE}^T)$ . This map may be compared to the RMS difference described above (Figures 5b–9b) to determine consistency of the reconstruction’s estimated error estimate. These statistics may be

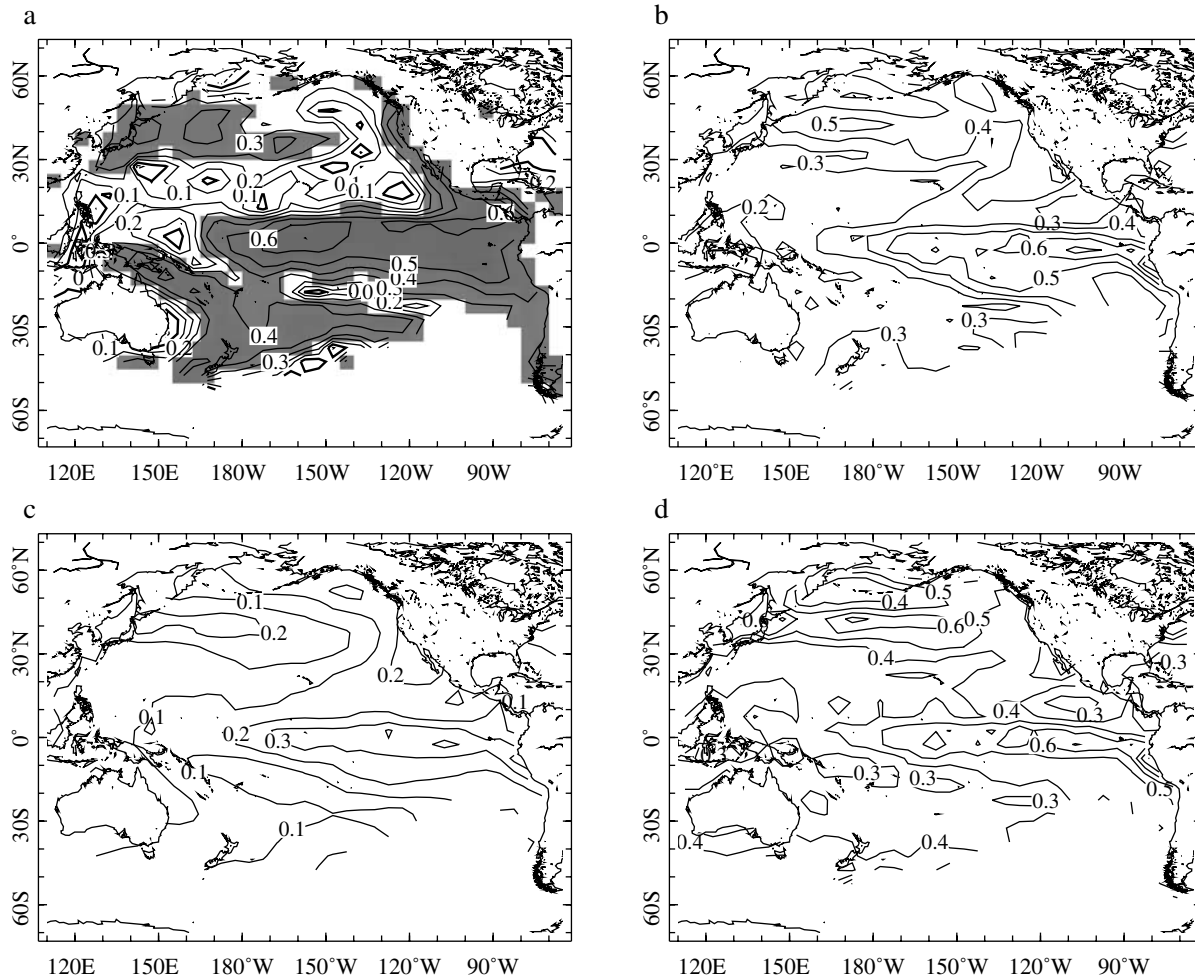


**Figure 6.** Verification (1856–1922) statistics for the coral-based SST reconstruction (CoSSTa). (a–d) Same as Figures 5a–5d.

compared between calibration and verification periods to determine whether there is artificially calibrated skill, and to explore the extent to which prior assumptions are violated.

[21] Calibration (1923–1990) statistics for the CoSSTa are shown in Figure 5. The correlation map (Figure 5a) shows that the reconstruction calibrates variance in the central and eastern equatorial Pacific as well as in the north and south subtropical gyres. RMS error between CoSSTa and KaSSTa is also largest in the central and eastern equatorial Pacific. This is because of the significant error in the calibration. Since the errors are large, the reconstructed variance is small, and there are large errors even where skill is high. This is illustrated by Figure 5c, which shows that the amplitude of reconstructed SST variability in the central and eastern equatorial Pacific is about the magnitude of the error in this region. Figure 5d shows the estimated error in the reconstruction; since these results are computed for the calibration period, it matches by design the actual error in the reconstruction over this period, with small differences due to the changes in data availability over this period.

### 3.5. Verification

#### 3.5.1. Comparison with withheld historical observations.

[22] The 1856–1922 statistics show that features of SST variability in the central and eastern equatorial Pacific are

verifiably resolved by the reconstruction (Figure 6a), with actual mean error (Figure 6b) similar to the estimated error (Figure 6d), albeit with small signal variance (Figure 6c). Skill is significant not only at the coral locations but in broad regions of the eastern equatorial Pacific as well and, to a lesser extent, in the subtropical gyres. An experiment with switched calibration and verification periods gives similar results (not shown). Use of one or three patterns (instead of two) for reconstruction shows slightly poorer verification skill. Because the analysis is punished for putting too much weight into patterns which do not contribute much to modern climate variability, overcalibration problems are minimized. These results suggest that our assumptions (section 2.3.1) on the stability of the calibration, number of patterns calibrated, and estimation of prior covariances, although violated in practice, are not fatal to the results, given the caveats discussed.

[23] These results also illustrate the globality of the methodology employed here (section 2): corals remote from these locales and even those from outside of the Pacific Basin (e.g., MAH, ABR, AQ19, CEB, MAD, ESP, and CAL) make significant contribution to the reconstruction skill, as judged by the correlation between individual coral records and time series of the calibrated patterns [Evans *et al.*, 2000, Table 3]. However, with the reduction in data availability over time (Figure 4c) the variance resolved decreases, and the error in the analysis increases. On the basis of these results,

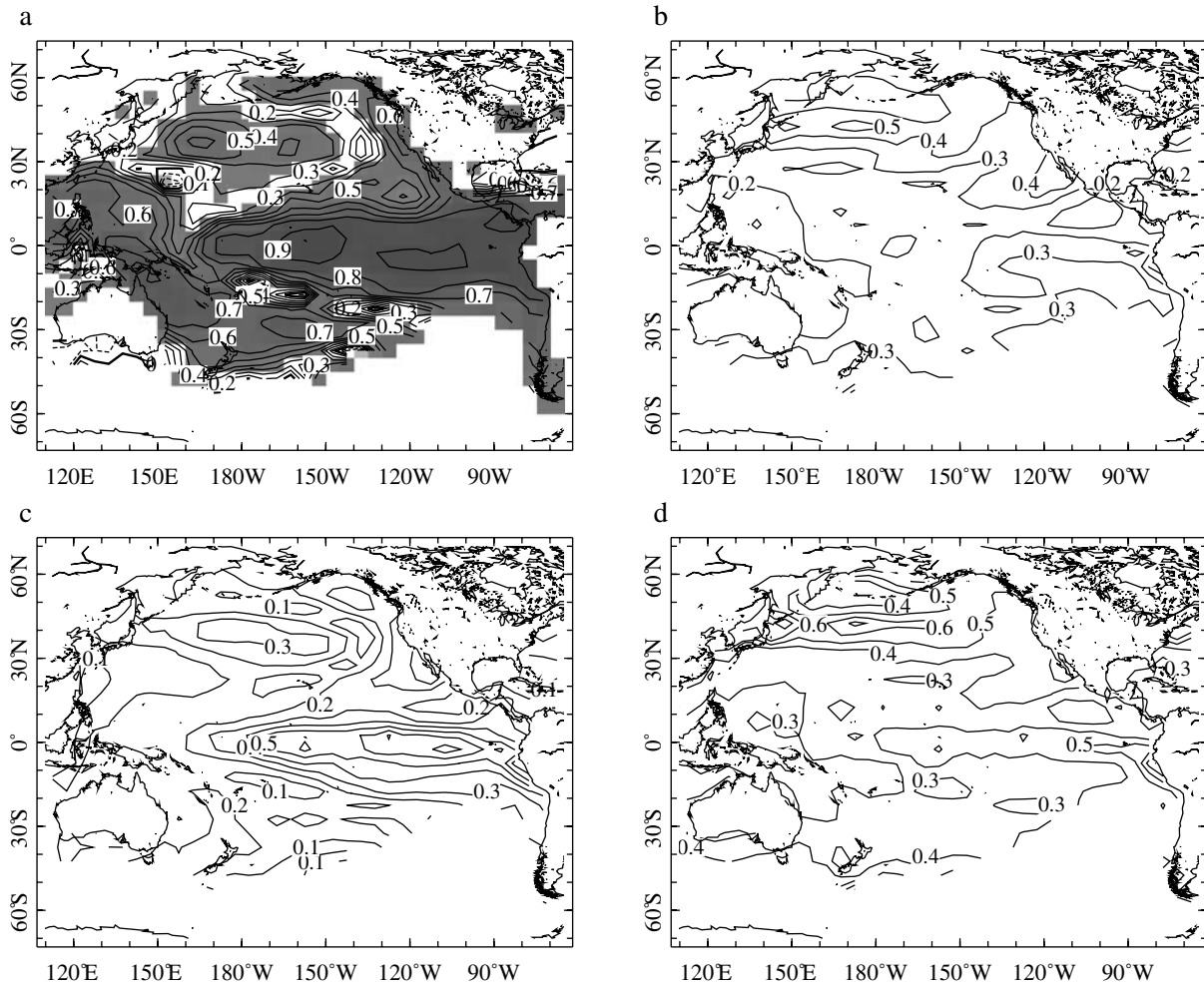


**Figure 7.** Verification (1856–1922) statistics for the benchmark SST reconstruction (see text). (a–d) Same as Figures 5a–5d.

we believe that the reconstruction is interpretable back to  $\sim 1800$  and is most skillful in the NINO3.4 index region ( $170^{\circ}$ – $120^{\circ}$ W,  $5^{\circ}$ N– $5^{\circ}$ S).

[24] Results also suggest that age model errors in individual coral records may not have much influence on the reconstruction results. Suspected problems with the age model of the Urvina Bay record of *Dunbar et al.* [1994] are not a large component of the reconstruction error: with the Urvina Bay record removed from the experiment, verification correlation with historical SST (as in Figure 6) changes by less than a tenth of a correlation unit in the most skillfully resolved regions (results not shown). The methodology employed here ((4)–(7)) ensures that the influence of any individual record is weighted by its observational uncertainty and that no one proxy record inordinately dominates the solution. More comprehensive experiments such as this may lead to improved observational error estimates for individual corals. They also highlight the importance of record replication to reduce overall proxy and reconstruction errors [Evans *et al.*, 1998].

[25] The reconstruction of the NINO3.4 index presented here is an improvement on that obtained via linear regression of the NINO3.4 SST index on the same 13 coral time series (Table 2). Calibration correlations retrieved by the two approaches are about equal; however, correlation with the NINO3.4 index of *Kaplan et*

*al.* [1998] shows that our reconstructed NINO3.4 index is more robust in the verification period. Verification period error rises only a small amount from the calibration period error, while the multiple linear regression error rises substantially. These results illustrate that limiting the reconstruction to what may be verified (space reduction) and incorporating calibration error into the reconstruction methodology (objectivity) improves the quality of the outcome.

**3.5.2. Comparisons with reconstructions based on synthetic data.** [26] We perform two additional experiments to assess the quality of the results. The first is reconstruction of the SST field using KaSSTa time series from the coral locations. This “benchmark” experiment is intended to illustrate reconstruction from the best possible data. A second experiment (“noise”) employs red noise time series with autocovariance statistics like those of the coral data and is intended to illustrate the influence of data containing no climatic information aside from persistence.

[27] The verification (1856–1922) results for these experiments are shown in Figures 7 and 8, respectively. Compared to CoSSTa, the benchmark reconstruction (Figure 7) has higher skill, smaller estimated error, and greater resolved variance. This is not surprising given the multivariate dependencies of  $\delta^{18}\text{O}$  and the higher uncertainties of individual  $\delta^{18}\text{O}$  time series. However, we also note

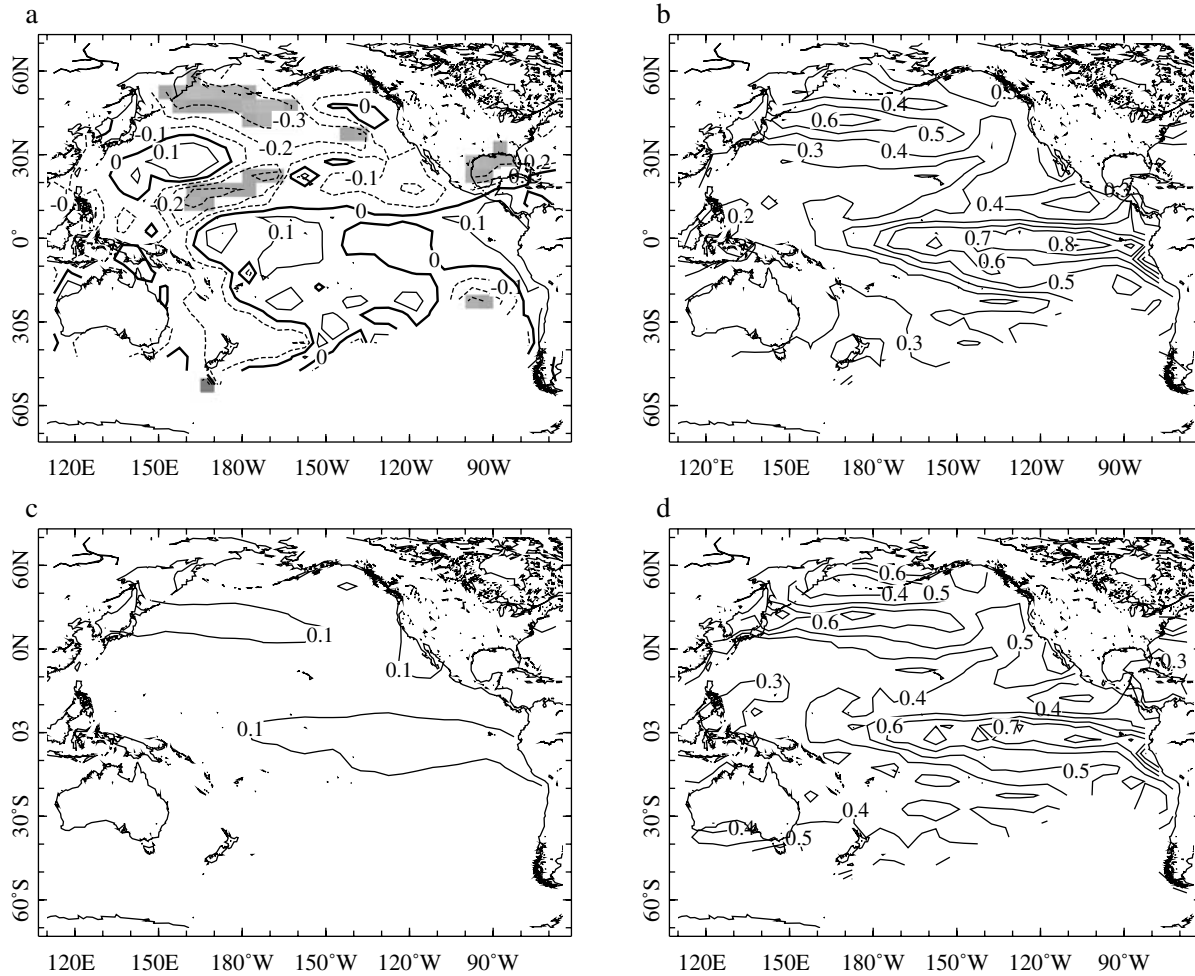


**Figure 8.** Verification (1856–1922) statistics for the noise SST reconstruction (see text). (a–d) Same as Figures 5a–5d.

(Figure 8) that the skill, resolved variance, and error in CoSSTa are better than that expected if the proxy data contained no climatic information whatsoever. These results suggest that additional proxy time series from important regions like the central and eastern equatorial Pacific will improve CoSSTa by resolving the reconstructed patterns with less error [Evans *et al.*, 1998].

### 3.5.3. Comparison with other ENSO reconstructions.

[28] A further and desirable verification is that our reconstruction agrees with similar attempts using different methodologies and proxy data sets. Two examples are the wintertime Southern Oscillation Index (SOI, difference between standardized sea level pressure anomalies at Tahiti and Darwin) reconstructed from tree ring data by *Stahle et al.* [1998] and the annual NINO3 SST index (SST anomaly averaged over 150°–90°W, 5°N–5°S) reconstructed from a variety of proxy data by *Mann et al.* [1998]. Rigorous intercomparison efforts are hindered by differences in the reconstructed variable, reconstructed season or year definition, selected calibration interval, and the overlap between proxy data sets employed. Nevertheless, given that the methods applied in these studies are all forms of multiple linear regression and use annual or higher-resolution proxy observations and that the reconstructed quantities (NINO3.4, NINO3, and SOI) are strongly covariant in the modern observations, it is a useful exercise to compare the results.

[29] Twentieth century correlations between all ENSO paleoestimates and instrumental indices are significant at or above the 95% level (Table 3, top). A stricter test is intercomparison of reconstructions over the nineteenth century (Table 3, bottom). Notably, two of the three proxy-proxy correlations remain significant, but this is not surprising because of common proxy data input. For example, 7 of the 14 time series employed by *Stahle et al.* [1998] are used by *Mann et al.* [1998], and 4 of 5–10 coral  $\delta^{18}\text{O}$  records employed in the present study (Figure 4) were also used in the study of *Mann et al.* [1998]. Only the *Stahle et al.* [1998] study and the present work are based on independent sets of proxy observations; correlation between these proxy ENSO reconstructions weakens from  $-0.61$  in the twentieth century to  $-0.09$  in the nineteenth century. While it should be noted that the agreement between these two paleoreconstructions improves through the nineteenth century, as number of corals available for analysis increases, this is discouragingly consistent with the results of *Schmutz et al.* [2000] regarding proxy North Atlantic Oscillation reconstructions. Disagreement is probably due to the small number of proxy observations available for the most important ENSO-influenced regions and proxy data age model error. Additional sites and more replication of data series will be required for better observational error estimates and improved reconstructions. Further improvements may also stem from systematic proxy-

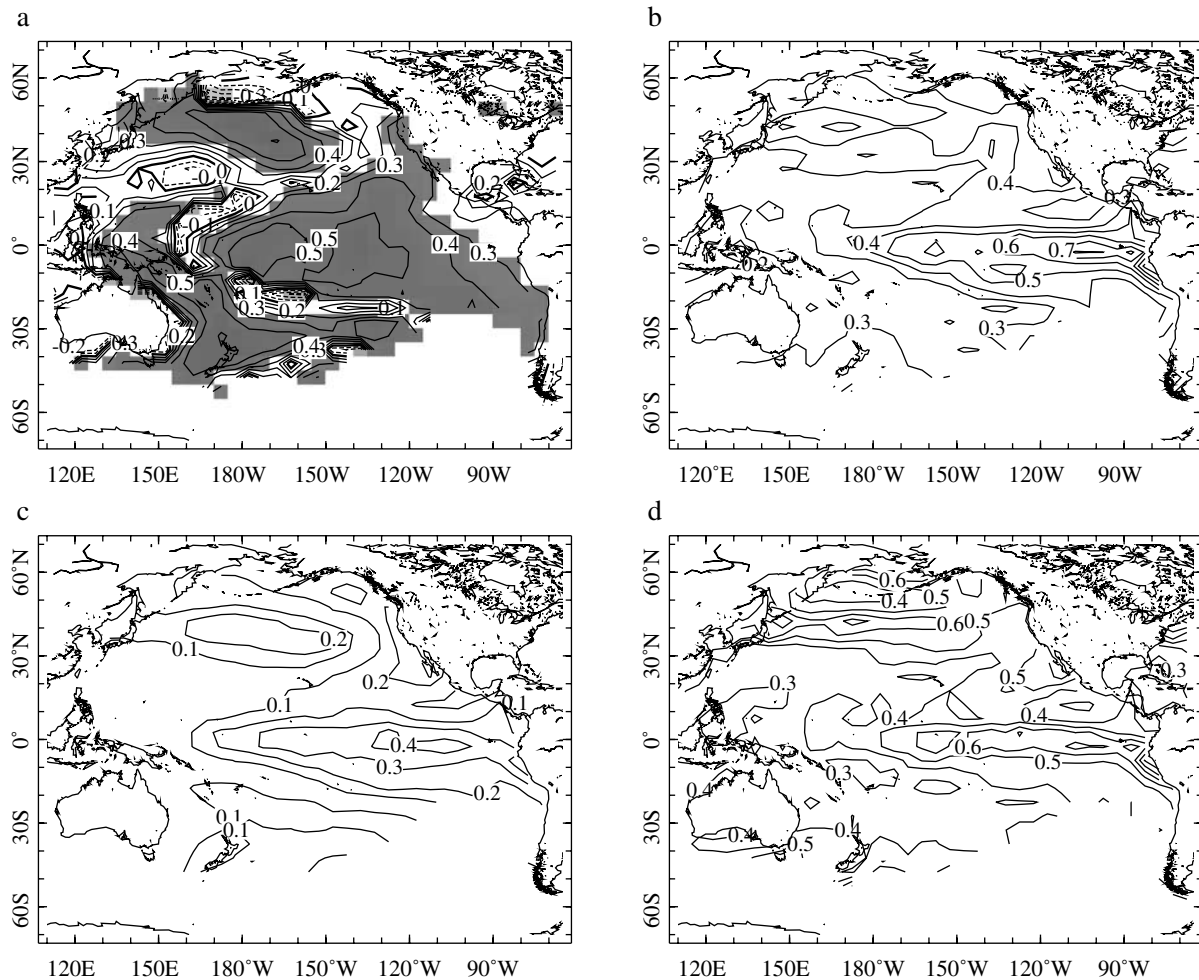


**Figure 9.** Verification (1856–1922) statistics for the tree ring indicator-based SST reconstruction (TrSSTa). Correlations significant at the 95% confidence level assuming 40 degrees of freedom are shaded. (a–d) Same as Figures 5a–5d.

instrumental and proxy-proxy intercomparison efforts as well as detailed study of the processes controlling proxy responses to climate variation.

## 4. Discussion

### 4.1. Reconstruction Features

[30] The CoSSTa reconstruction presented here is based on at most 13 corals, which together resolve at most two patterns of SST variability. The ENSO pattern of SST variability is resolved much

**Table 2.** Skill of NINO3.4 Estimates, 1856–1990<sup>a</sup>

Statistic	NINO3.4 (This study)	NINO3.4 (MLR)
Calibration correlation	0.83	0.84
Calibration error	0.45°C	0.35°C
Verification correlation	0.62	0.54
Verification error	0.51°C	0.59°C

<sup>a</sup> Correlations and error estimates formed via comparison with Kaplan *et al.* [1998] NINO3.4. Calibration period: 1923–1990; verification period: 1856–1922. MLR, multiple linear regression.

more robustly than the second pattern; this is to be expected given that tropical sampling sites from the Pacific and Indian Oceans are expected to resolve ENSO [Evans *et al.*, 1998]. It is also consistent with the results of many of the coral researchers referenced here who find that their individual data series index ENSO quite reliably on interannual timescales. Correlation of the first pattern reconstructed here with the NINO3.4 SST index (SST anomaly average for the region 170°W–120°E, 5°N–5°S) from Kaplan *et al.* [1998] is 0.71 for the calibration (1923–1990) period and 0.62 for the verification (1856–1922), significant at the 99% level assuming 45 degrees of freedom [Trenberth, 1984]. The trend pattern reconstructed has a very small amplitude (Figures 3 and 4), much smaller than that found in many individual coral records. This is consistent with our finding [Evans *et al.*, 2000] that individual coral  $\delta^{18}\text{O}$  time series often have decadal and secular variability but that much of this variance does not linearly reflect SST variability or SST covariant variability in net freshwater flux. By analyzing the coral data as a set we can isolate the climatically induced fraction.

### 4.2. Comparison With Results Based on Tree Ring Data

[31] Results from CoSSTa may be compared to those obtained by Evans *et al.* [2001], which attempted reconstruction of the same target climate field using 15 tree ring indicators from Pacific

**Table 3.** Comparison of ENSO Paleoreconstructions<sup>a</sup>

Correlation $r$	M-NINO3	E-NINO3.4	K-NINO3	K-SOI
		1801–1900		
S-SOI	–0.30 <sup>b</sup>	–0.09	–0.55 <sup>b</sup>	0.56 <sup>b</sup>
M-NINO3		0.60 <sup>b</sup>	0.69 <sup>b</sup>	–0.46 <sup>b</sup>
E-NINO3.4			0.53 <sup>b</sup>	–0.32
K-SOI				–0.70 <sup>b</sup>
		1901–1990		
S-SOI	–0.45 <sup>b</sup>	–0.61 <sup>b</sup>	–0.75 <sup>b</sup>	0.78 <sup>b</sup>
M-NINO3		0.67 <sup>b</sup>	0.62 <sup>b</sup>	–0.45 <sup>b</sup>
E-NINO3.4			0.81 <sup>b</sup>	–0.66 <sup>b</sup>
K-SOI				–0.76 <sup>b</sup>

<sup>a</sup> Comparisons with K-NINO3 in 1801–1900 period are for 1856–1990, and comparisons with K-SOI are for 1866–1990. Sources: M-NINO3, *Mann et al.* [1998]; E-NINO3.4, this study; K-NINO3, *Kaplan et al.* [1998]; S-SOI, *Stahle et al.* [1998]; K-SOI, *Können et al.* [1998].

<sup>b</sup> Correlations are significant at or above the 95% confidence level (considering effects of serial autocorrelation in the time series [*Trenberth*, 1984]).

influenced regions of North and South America. The tree ring indicators were selected by *Villalba et al.* [2001] because they sense local precipitation and temperature anomalies which are in turn associated with Pacific Basin SST variability. In this work we found that the tree ring indicators could be used to reconstruct one pattern of SST variability. On the basis of data availability and error estimates we believe this reconstruction, here termed TrSSTa, is interpretable for the interval 1600–1990 (Figure 9). This pattern is spatially ENSO-like [*Villalba et al.*, 2001; *Evans et al.*, 2001] but is not as equatorially trapped as ENSO is. Also, unlike the ENSO pattern, its dominant frequency of variability is broadly decadal to interdecadal.

[32] Caveats that should be considered here are that both proxy data sets are small, the number of resolved patterns is small, and the errors in the reconstructions are quite large. Nevertheless, it appears that these two independent sources of proxy data resolve SST variability which is roughly separable in the frequency domain (Figure 10). It may be possible to reconstruct all three patterns with skill from the combined data sets if the observational error for the different proxies (equation (4)) can be accurately determined. However, we also note that both proxy

reconstructions contain much more variance at low frequencies than do historical observations. Furthermore, the two proxy reconstructions suggest differing levels of interdecadal variability. Multiproxy reconstructions, in which the type of proxy data employed changes over time, may reflect spurious frequency evolution due to skill partitioning in the frequency domain. Reconstruction experiments in which subsets of proxy data are sequentially removed from the analysis may indicate whether this problem is significant.

#### 4.3. Low-Frequency Behavior of ENSO in the Preindustrial Era

[33] Since CoSSTa has verifiable skill only in certain parts of the reconstruction domain (Figure 6), we form an area-average index for time series analysis from a region where skill is high. As suggested by Figure 6 we examine characteristics of the NINO3.4 SST index formed from CoSSTa. The uncertainty in CoSSTa is such that it precludes sophisticated quantitative analyses. Nevertheless, the results suggest that ENSO was more frequent after 1980, lower in the 1940–1975 epoch, and again more frequent

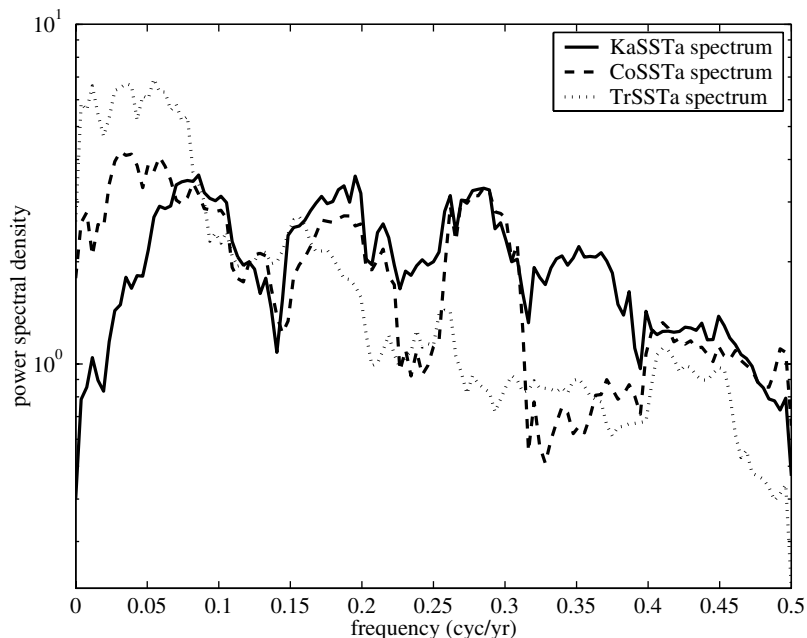


**Figure 10.** Power spectra of KaSSTa, CoSSTa, and TrSSTa over the common interval 1856–1990.

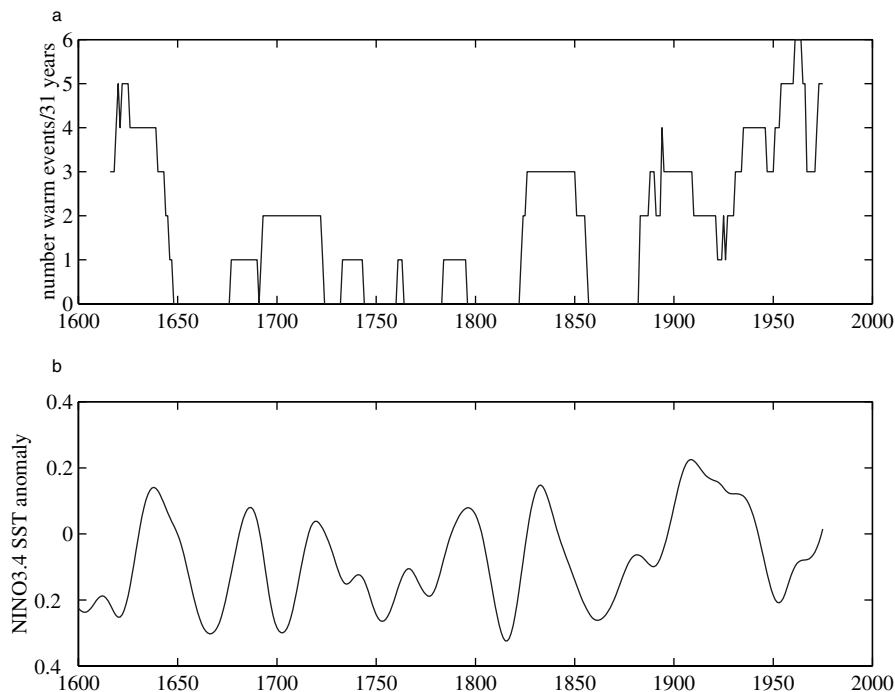


**Figure 11.** (a) Number of ENSO warm phase events (NINO3.4 SST anomaly  $>0.5^{\circ}\text{C}$  relative to the mean over a running 31 year window), as reconstructed in CoSSTa. (b) TrSSTa NINO3.4 SST anomaly ( $^{\circ}\text{C}$ ), filtered with a 31 year Hanning window. On the basis of error analysis and number of proxy time series available, TrSSTa is interpretable back to 1550; CoSSTa is interpretable back to about 1807.

around the beginning of the 1900s. This is consistent with previous work by Trenberth and Shea [1987] and confirmed later by coral paleoclimate studies [Cole *et al.*, 1993; Urban *et al.*, 2000]. CoSSTa NINO3.4 further suggests that the 1820–1860 period was also a period of relatively vigorous ENSO activity, while the 1860–1880 period was relatively quiescent (Figure 11), the very strong event of 1877 excepted. Comparison with Pacific decadal SST variability inferred independently from TrSSTa suggests that ENSO warm phase frequency is associated with periods of warm Pacific mean state, consistent with the hypothesis put forward by Gershunov and Barnett [1998] and Urban *et al.* [2000]. As these observations extend at least into the preindustrial period, attribution of the unusually ENSO-rich past few decades may lie in part with natural variability.

## 5. Conclusions

[34] We have applied a methodology to verifiably reconstruct past climate variability from proxy data to the problem of SST field reconstruction using the available network of coral  $\delta^{18}\text{O}$

data. Two patterns are reconstructed: ENSO and a trend in which regions of the North Pacific and eastern equatorial Pacific respond in the opposite sense. The reconstruction has large errors but is probably qualitatively interpretable back into the early nineteenth century. A similar attempt to reconstruct Pacific SST using an independent set of tree ring indicators suggests that these different types of proxy data may provide reconstruction skill roughly separable in the frequency domain. Comparison of the results of these two reconstructions of Pacific Basin SST suggests that the frequency of ENSO is tied to the mean state of the Pacific, that said frequency fluctuates on interdecadal time scales, and that this association extends into the preindustrial era. If these observations are correct, they will be borne out and strengthened by the incorporation of additional paleoproxy data into the analysis.

[35] **Acknowledgments.** This work was supported by NOAA/ESH grant NA86GP0437 and NOAA/CCDD grant NA16GP1616. We thank Mark Eakin, the WDC-A for Paleoclimatology, and the cited scientists for the use of their data. LDEO contribution 6257.

## References

- Bennett, A. F., Inverse methods in assessing ship-of-opportunity networks and estimating circulation and winds from tropical expendable bathythermograph data, *J. Geophys. Res.*, *95*, 16,111–16,148, 1990.
- Bretherton, C. S., C. Smith, and J. M. Wallace, An intercomparison of methods for finding coupled patterns in climate data, *J. Clim.*, *5*, 541–560, 1992.
- Bretherton, F. P., and J. C. McWilliams, Estimations from irregular arrays, *Rev. Geophys.*, *18*, 789–812, 1980.
- Cane, M. A., A. Kaplan, R. N. Miller, B. Tang, E. C. Hackert, and A. J. Busalacchi, Mapping tropical Pacific sea level: Data assimilation via a reduced state space Kalman filter, *J. Geophys. Res.*, *101*, 22,599–22,617, 1996.
- Cane, M. A., A. C. Clement, A. Kaplan, Y. Kushnir, R. Murtugudde, D. Pozdnyakov, R. Seager, and S. E. Zebiak, 20th century sea surface temperature trends, *Science*, *275*, 957–960, 1997.
- Charles, C. D., D. E. Hunter, and R. G. Fairbanks, Interaction between the ENSO and the Asian monsoon in a coral record of tropical climate, *Science*, *277*, 925–928, 1997.
- Cole, J. E., R. G. Fairbanks, and G. T. Shen, Recent variability in the Southern Oscillation: Isotopic results from a Tarawa Atoll coral, *Science*, *260*, 1790–1793, 1993.
- Cook, E. R., K. R. Briffa, and P. D. Jones, Spatial regression methods in dendroclimatology—A review and comparison of 2 techniques, *Int. J. Clim.*, *14*, 379–402, 1994.
- Druffel, E. R. M., and S. Griffin, Large variations of surface ocean radiocarbon: Evidence

- of circulation changes in the southwestern Pacific, *J. Geophys. Res.*, *98*, 20,246–20,259, 1993.
- Dunbar, R. B., G. M. Wellington, M. W. Colgan, and P. W. Glynn, Eastern Pacific sea surface temperature since 1600 A.D.: The  $\delta^{18}\text{O}$  record of climate variability in Galápagos corals, *Paleoceanography*, *9*, 291–315, 1994.
- Evans, M. N., A. Kaplan, and M. A. Cane, Optimal sites for coral-based reconstruction of sea surface temperature, *Paleoceanography*, *13*, 502–516, 1998.
- Evans, M. N., R. G. Fairbanks, and J. L. Rubenstone, The thermal oceanographic signal of El Niño reconstructed from a Kiriritimati Island coral, *J. Geophys. Res.*, *104*, 13,409–13,421, 1999.
- Evans, M. N., A. Kaplan, and M. A. Cane, Intercomparison of coral oxygen isotope data and historical sea surface temperature (SST): Potential for coral-based SST field reconstructions, *Paleoceanography*, *15*, 551–562, 2000.
- Evans, M. N., A. Kaplan, M. A. Cane, and R. Villalba, Globality and optimality in climate field reconstructions from proxy data, in *Interhemispheric Climate Linkages*, edited by V. Markgraf, pp. 53–72, Cambridge Univ. Press, New York, 2001.
- Fritts, H. C., T. R. Blasing, B. P. Hayden, and J. E. Kutzbach, Multivariate techniques for specifying tree-growth and climate relationships and for reconstructing anomalies in paleoclimate, *J. Appl. Meteorol.*, *10*, 845–864, 1971.
- Gandin, L. S., *Objective Analysis of Meteorological Fields*, translated from Russian, Isr. Program for Sci. Transl., Jerusalem, 1965.
- Gershunov, A., and T. P. Barnett, Interdecadal modulation of ENSO teleconnections, *Bull. Am. Meteorol. Soc.*, *79*, 2715–2725, 1998.
- Glantz, M. H., R. W. Katz, and N. Nicholls, *Scientific Basis and Societal Impact*, Cambridge Univ. Press, New York, 1990.
- Hansen, J., and S. Lebedeff, Global surface air temperatures: Update through 1987, *J. Geophys. Res.*, *92*, 13,345–13,372, 1988.
- Heiss, G. A., Coral reefs in the Red Sea: Growth, production and stable isotopes, *Tech. Rep. 32*, GEOMAR 1994.
- Hurrell, J. W., Decadal trends in the North-Atlantic Oscillation—Regional temperatures and precipitation, *Science*, *269*, 676–679, 1995.
- Hurrell, J. W., and K. E. Trenberth, Global sea surface temperature analyses: Multiple problems and their implications for climate analysis, modeling and reanalysis, *Bull. Am. Meteorol. Soc.*, *80*, 2661–2678, 1999.
- Jones, P. D., T. J. Osborn, and K. R. Briffa, Estimating sampling errors in large-scale temperature averages, *J. Clim.*, *10*, 2548–2568, 1997.
- Kaplan, A., Y. Kushnir, M. A. Cane, and M. B. Blumenthal, Reduced space optimal analysis for historical datasets: 136 years of Atlantic sea surface temperatures, *J. Geophys. Res.*, *102*, 27,835–27,860, 1997.
- Kaplan, A., M. A. Cane, Y. Kushnir, A. C. Clement, M. B. Blumenthal, and B. Rajagopalan, Analyses of global sea surface temperature 1856–1991, *J. Geophys. Res.*, *103*, 18,567–18,589, 1998.
- Kaplan, A., Y. Kushnir, and M. A. Cane, Analysis of historical sea level pressure 1854–1992, *J. Clim.*, *13*, 2987–3002, 2000.
- Kaplan, A., M. A. Cane, and Y. Kushnir, Reduced space approach to the optimal analysis of historical marine observations: Accomplishments, difficulties, and prospects, in *WMO Guide to the Applications of Marine Climatology*, World Meteorol. Org., Geneva, Switzerland, in press, 2002.
- Können, G. P., P. D. Jones, M. H. Kaltofen, and R. J. Allan, Pre-1866 extensions of the Southern Oscillation Index using early Indonesian and Tahitian meteorological readings, *J. Clim.*, *11*, 2325–2339, 1998.
- Lawley, D. N., Tests of significance for the latent roots of covariance and correlation matrices, *Biometrika*, *43*, 128–136, 1956.
- Linsley, B. K., R. B. Dunbar, G. M. Wellington, and D. A. Mucciarone, A coral-based reconstruction of Intertropical Convergence Zone variability over Central America since 1707, *J. Geophys. Res.*, *99*, 9977–9994, 1994.
- Mann, M. E., R. S. Bradley, and M. K. Hughes, Global temperature patterns over the past five centuries: Implications for anthropogenic and natural forcing of climate, *Nature*, *392*, 779–787, 1998.
- Mardia, K. V., J. T. Kent, and J. M. Bibby, *Multivariate Analysis*, Academic, San Diego, Calif., 1979.
- Parker, D. E., P. D. Jones, C. K. Folland, and A. Bevan, Interdecadal changes of surface temperature since the late nineteenth century, *J. Geophys. Res.*, *99*, 14,373–14,399, 1994.
- Patzöld, J., Growth rhythms recorded in stable isotopes and density bands in the reef coral *Porites lobata* (Cebu, Philippines), *Coral Reefs*, *3*, 87–90, 1984.
- Philander, S. G. H., *El Niño, La Niña, and the Southern Oscillation*, Academic, San Diego, Calif., 1990.
- Quinn, T. M., F. W. Taylor, and T. J. Crowley, A 173 year stable isotope record from a tropical South Pacific coral, *Quat. Sci. Rev.*, *12*, 407–418, 1993.
- Quinn, T. M., T. M. Crowley, F. W. Taylor, C. Henin, P. Joannot, and Y. Join, A multicentury stable isotope record from a New Caledonia coral: Interannual and decadal sea surface temperature variability in the southwest Pacific since 1657 A.D., *Paleoceanography*, *13*, 412–426, 1998.
- Rao, C. R., *Linear Statistical Inference and Its Applications*, John Wiley, New York, 1973.
- Ropelewski, C. F., and M. S. Halpert, Global and regional scale precipitation patterns associated with the El Niño/Southern Oscillation, *Mon. Weather Rev.*, *114*, 2352–2362, 1987.
- Schmutz, C., J. Luterbacher, D. Gyalistras, E. Xoplacki, and H. Wanner, Can we trust proxy-based NAO index reconstructions?, *Geophys. Res. Lett.*, *27*, 1135–1138, 2000.
- Schneider, T., Analysis of incomplete climate data: Estimation of mean values and covariance matrices and imputation of missing values, *J. Clim.*, *14*, 853–871, 2001.
- Shen, G. T., J. E. Cole, D. W. Lea, L. J. Linn, T. A. McConnaughey, and R. G. Fairbanks, Surface ocean variability at Galápagos from 1936–1982: Calibration of geochemical tracers in corals, *Paleoceanography*, *7*, 563–588, 1992.
- Stahle, D. W., et al., Experimental dendroclimatic reconstruction of the Southern Oscillation, *Am. Meteorol. Soc. Bull.*, *79*, 2137–2152, 1998.
- Trenberth, K. E., Some effects of finite sample size and persistence on meteorological statistics, part I, Autocorrelations, *Mon. Weather Rev.*, *112*, 2359–2379, 1984.
- Trenberth, K. E., and D. J. Shea, On the evolution of the Southern Oscillation, *Mon. Weather Rev.*, *115*, 3078–3096, 1987.
- Tudhope, A. W., G. B. Shimmield, C. P. Chilcott, M. Jebb, A. E. Fallick, and A. N. Dalgleish, Recent changes in climate in the far western equatorial Pacific and their relationship to the Southern Oscillation: Oxygen isotope records from massive corals, *Earth Planet. Sci. Lett.*, *136*, 575–590, 1995.
- Urban, F. E., J. E. Cole, and J. T. Overpeck, Influence of mean climate change on climate variability from a 155-year tropical Pacific coral record, *Nature*, *392*, 779–787, 2000.
- Villalba, R., R. D. D'Arrigo, E. R. Cook, G. Wiles, and G. C. Jacoby, Decadal-scale climatic variability along the extra-tropical western coast of the Americas over past centuries inferred from tree-ring records, in *Interhemispheric Climate Linkages*, edited by V. Markgraf, pp. 155–172, Cambridge Univ. Press, New York, 2001.
- Wallace, J. M., Observed climatic variability: Time dependence, in *Decadal Climate Variability: Dynamics and Predictability*, NATO ASI Ser., Ser. I, vol. 44, pp. 1–30, Springer-Verlag, New York, 1996a.
- Wallace, J. M., Observed climatic variability: Spatial structure, in *Decadal Climate Variability: Dynamics and Predictability*, NATO ASI Ser., Ser. I, vol. 44, pp. 31–81, Springer-Verlag, New York, 1996b.
- White, W. B., and R. G. Peterson, An Antarctic circumpolar wave in surface pressure, wind, temperature and sea-ice extent, *Nature*, *380*, 699–702, 1996.
- Zhang, Y., J. M. Wallace, and D. S. Battisti, ENSO-like interdecadal variability: 1900–93, *J. Clim.*, *10*, 1004–1020, 1997.

M. A. Cane and A. Kaplan, Lamont-Doherty Earth Observatory, Route 9W, Palisades, NY 10964, USA.

M. N. Evans, Laboratory of Tree-Ring Research, University of Arizona, 105 West Stadium, Tucson, AZ 85721, USA. (mevans@lrr.arizona.edu)